RESEARCH ON PHOTOELECTRIC TRACKING CONTROL SYSTEM OF SUBMARINE BASED ON FRACTIONAL ORDER PID DISTURBANCE OBSERVER

Zongkai Liu[1,2], Yuheng Zhang[1,3*], Yuming Liu[1,3]

When the submarines moving underwater, the submarine-based photoelectric tracking control systems will be affected by the nonlinear disturbance that may come from the uncertainty pressure pulsation originated from the wave or the submarine propeller. These effects make tracking accuracy of the photoelectric tracking system become worse. Therefore, in this study, a Fractional Order PID (FOPID) disturbance observer control method is proposed, and the disturbance observer is designed to eliminate uncertain disturbance. The robustness and stability of the control system are guaranteed by fractional PID. The whole control system is designed by combining the compound axis of fast steering mirror (FSM) and fractional order PID (FOPID) disturbance observer (DOB) controller. Then the CFX numerical simulation is carried out to simulate the navigation of submarine model in the flow field at Reynolds number $Re=10^7$, and the disturbance effect of propeller on the carrier is analyzed in the simulation. The azimuth error is stable within ± 0.8 mrad, and the pitching error is stable among ± 0.6 mrad.

Keywords: Photoelectric tracking system, Fractional Order PID, Disturbance observer, Near surface submarine disturbance

1. Introduction

Photoelectric tracking system is a comprehensive photoelectric system, which is widely used in reconnaissance, photoelectric countermeasure, counteracting aircraft target and precise measurement [1][2]. Due to the influence of wave, wind and other factors, the photoelectric equipment should move with the ship, which greatly reduce the accuracy of target acquisition and tracking. In addition, when the submarine moving underwater, the sea water around the submarine will form vortex streets. The generation and separation of vortex streets will induce the hull vibration. For the higher Reynolds number, turbulence will form much complex vortexes around the hull. The turbulence's evolution is more random, causing more complex fluctuation. This kind of disturbance will eventually react to the photoelectric tracking system on the carrier, it will affect

[1] Nanjing University of Science and Technology, School of Automation, Nanjing 210094, China
[2] Nanjing Yuebo Power System Co., LTD, Nanjing 210008, China
[3] The 28th Research Institute of China Electronics Technology Group Corporation, Nanjing 210007, China; *Corresponding author. E-mail: 973628404@qq.com

the tracking accuracy of photoelectric tracking system.

The integer order PID control system is included in the fractional order. By adding orders to the differential and integral terms, the fractional order can be adjusted in a wider field. Therefore, the fractional order controller can also be utilized in integer order controller. At the same time, compared with the PID control, it appears a get better control effect. It has been widely used in the magnetic suspension position control[3] liquid level servo control[4], motor control[5], permanent-magnet synchronous generator[6] and unmanned aerial vehicle (UAV) roll control study[7].

A closed loop controlled nominal model can be established by the disturbance observers, which can feedback the system's output error to the original system by a feed forward compensation. This method can suppress the errors from the moment distribution or model uncertainty. The disturbance observer also be applied on the liquid level servo control[8]. In references[9], the disturbance observer adaptive sliding mode control not only can increase the robustness but also can reduce the chattering effect. The disturbance observer is used for improving the tracking accuracy and reducing the interference in the self-balancing robot[10], which offers several advantages such as reducing the interference in the multi input and multi output control system[11]. Both the disturbance observer and the fractional PID control have been utilized in the other researches, such as the permanent magnet synchronous generator [12].

In this paper, the fractional order PID and disturbance observer are applied to reduce the effect of torque disturbance in the photoelectric tracking control system of submarine. And the fluid dynamics disturbance characters of submarine are numerical simulated by CFX fluid calculation software. Combined with the simulation results, the designed control system is tested when the underwater disturbance acts on submarine. The simulation results show that this control method is better than the traditional control model.

2. Design of compound axis control system

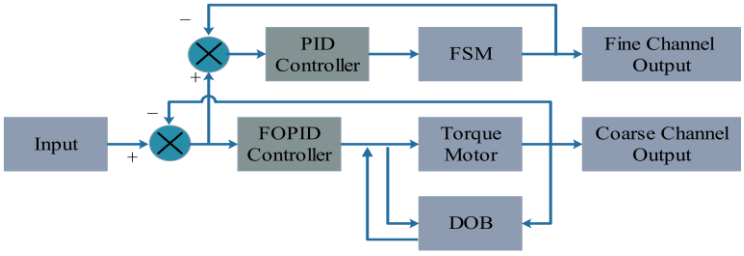

Fig. 1. The system block diagram of compound axis control

Fig. 1 displays the compound axis control system, which consists with the coarse and fine two channels tracking control sub-systems. The coarse channel

torque motor tracking control system is adjusted by the fractional order PID disturbance observer (FOPID) controller so as to eliminate the influence of common friction torque and improve the turntable tracking accuracy. The fine channel fast steering mirror controlled by PID controller to precisely adjust optical axis pointing to eliminate the final residual error. Moreover, the compound axis control system's error depends on the two channels independent control systems and equals to the product of two channels' error.

2.1. Design of the fractional PID disturbance observer control for the coarse tracking system

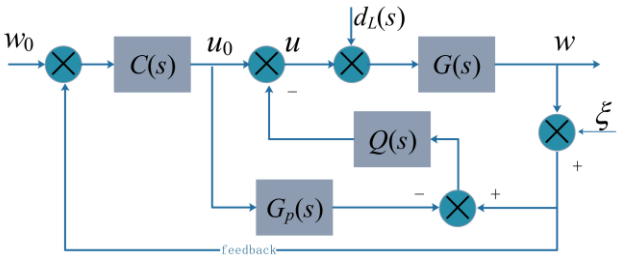

Fig. 2. The block diagram of disturbance observer used in this study

Fig. 2 is design of the fractional PID disturbance observer control for the coarse tracking system. d_L is the friction torque also the external interference of the controlled object motor, ξ is the measurement noise produced by the system sensor, $\hat{d}$ is the other interference observed by the $Q(s)$. w_0 is the expected input set for the system, $C(s)$ is the fractional order PID controller, $G(s)$ is the controlled object in the system, $G_p(s)$ is nominal model of the disturbance observer, $Q(s)$ is filter module of the disturbance observer.

2.1.1. Design of the low pass filter of disturbance observer

The design of filter proposed by H. S. Lee is basic design method of filter designed in the disturbance observer[13]. $Q(s)$ can be expressed as:

$$Q(s)=\frac{\sum_{k=0}^{M} a_k(\tau s)^k}{(\tau s+1)^N} \tag{1}$$

In this formula, $a_k = N!/(N-k)!k!$ that N is the order of the filter denominator, M is the order of filter molecules, τ is time constant. It can be seen from the above analysis that the relative order of the filter can be obtained by $N-M$.

Suppose N=1, 2, 3, the filter with relative order 1 can be expressed as:

$$Q(s)=\frac{1}{(\tau s+1)}, \quad N=1 \tag{2}$$

$$Q(s)=\frac{2\tau s+1}{(\tau s+1)^2},\quad N=2 \tag{3}$$

$$Q(s)=\frac{6(\tau s)^2+3\tau s+1}{(\tau s+1)^3},\quad N=3 \tag{4}$$

Fig. 3 and Fig. 4 are the bode diagram of $Q(s)$ and $1-Q(s)$, supposing τ=0.001. The filter bandwidth becomes larger with the increase of N, which makes the system more insensitive to external disturbances. However, from the bode diagram of the filter when N=3, it is obvious that there is a fluctuation in the low frequency band, which means that the control system will be more sensitive to the measurement noise. When N=1, although there is no fluctuation in the Fig. 3, the ability of restraining external disturbance becomes worse due to the narrow bandwidth. During the process of practical application, the high order selection call for a high requirement of the system computing ability, leading to the more delay. So the basic standard of the order selection is to give priority to consider the achieving of the performance index, based on which the order selection should be as low as possible. So this study chooses N=2.

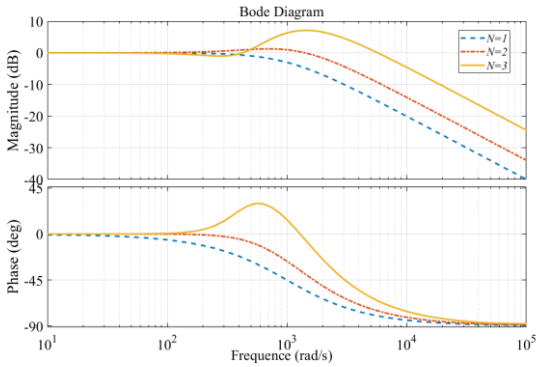

Fig. 3. τ=0.001 Bode diagram of $Q(s)$

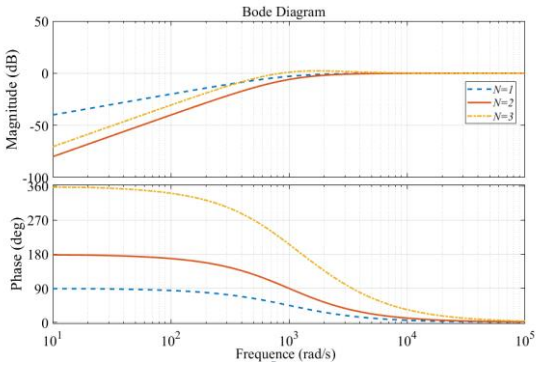

Fig. 4. τ=0.001 Bode diagram of $1-Q(s)$

As shown in Fig. 5 and Fig. 6 (supposing N=2, τ=0.001s, 0.01s, 0.1),

when the filter structure is determined, the time constant τ can also affect the filter bandwidth. When τ is small, the control system has better improvement effect on external interference (system robustness), but poor ability in the suppression of high-frequency noise. When τ is large, the control system has a worse improvement effect on external interference and the robustness, but appears a good effect on the suppression of the high frequency noise.

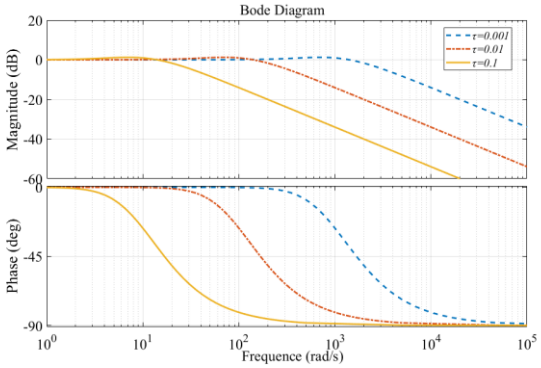

Fig. 5. N=2 Bode diagram of $Q(s)$

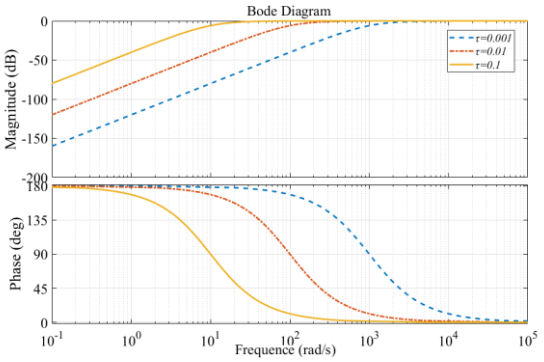

Fig. 6. N=2 Bode diagram of $1-Q(s)$

2.1.2. Design of Fractional Order PID controller

Firstly, the integrated time absolute error (ITAE) criterion is used as the optimal performance index, and the parameters k_p, k_d, k_i, λ, μ are optimized through the design interface of the optimal fractional order PID controller in MATLAB. These parameters were obtained by trial and error method. However, for the controlled object, the optimal fractional order PID controller designed in this way also has some limitations. So the parameters should be optimized with the simulation results.

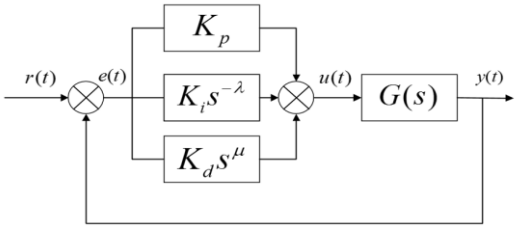

Fig. 7. The fractional $PI^{\lambda}D^{\mu}$ system block diagram

The transfer function of fractional order $PI^{\lambda}D^{\mu}$ controller can be expressed as:

$$G_c(s) = \frac{U(s)}{E(s)} = K_p + \frac{K_i}{s^{\lambda}} + K_d s^{\mu}; (0 < \lambda, \mu < 2) \tag{5}$$

So we can get the input and output expression of fractional order $PI^{\lambda}D^{\mu}$ controller in time domain:

$$u(t) = k_p e(t) + k_i D^{-\lambda} e(t) + k_d D^{\mu} e(t) \tag{6}$$

The $e(t) = r(t) - y(t)$ is the control system error, $r(t)$ is the expected position parameter of the controlled system, $y(t)$ is the output of the closed-loop system in the figure. $G_c(s)$ the controller of fractional order, as shown in Fig. 7, $G(s)$ is the transfer function of the controlled object. k_p, k_i, k_d are the proportional, integral and differential gain, respectively. λ and μ are fractional order factors of integral and differential terms. They can be set as $0 < \lambda, \mu < 2$, if the controller order is greater than 2, it is not traditional PID control and out of the discussion scope.

2.2. The design of the fast steering mirror control system

The FSM used in the fine channel tracking system is a P-T04K010 piezoelectric ceramic deflector made by PI company in Germany. Four moving fulcrums are built in the fast steering mirror to push the flexible platform of piezoelectric deflector to realize the fine adjustment of two degrees of pitch and tilt. The physical swing angle amplitude is ± 12.5mrad, while the closed-loop precision of P-T04K010 is $5\mu rad$. In the experiment, the frequency response curve of FSM in the closed-loop state measured and closed-loop transfer function by the spectrometer [14],[15]:

$$G(s) = \frac{1}{(0.0036+1)(2.53^{-6}s^2 + 0.0022s + 1)} \tag{7}$$

The simulation system diagram is as Fig. 8 shows:

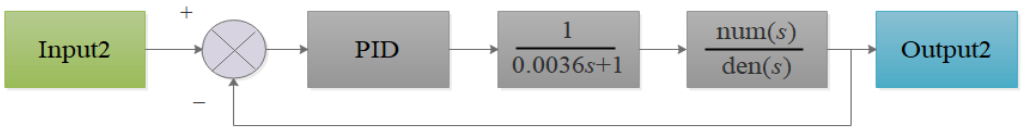

Fig. 8. Simulation diagram of the fine channel system (Has changed this figure)

When the tracking error of the coarse tracking input is small enough, the light path of the fast steering mirror can be more accurate. The input 2 is the output error of the coarse tracking channel. The driving element movement to realize the deflection of the fast steering mirror is controlled by PID controller. With the characteristic of the light weight and fast response, it can correct the light path in time and reduce the residual error of the coarse channel system.

2.3. Simulation analysis of compound axis

PID controller parameters in fine channel are $K_p = 3$, $K_i = 200$, $K_d = 0.01$. The fractional PID parameters in coarse channel are $k_p = 50$, $k_d = 20$, $\mu = 1.3685$, respectively. The nominal model is determined by current experiment and adjusted by Bode diagram. It set as $P(s) = 36.8/s$. Low pass filter parameters are $Q(s) = (2\tau s + 1)/(\tau s + 1)^2$, $\tau = 0.001$. Set the friction moment disturbance as $d_L = 0.2 + 0.1\sin(2\pi t)$/rad. The expected input of control system is 0 for numerical analysis. The tracking error of compound axis control is shown in Fig. 9, and the mean square value of tracking error is 1.82×10^{-3} mrad.

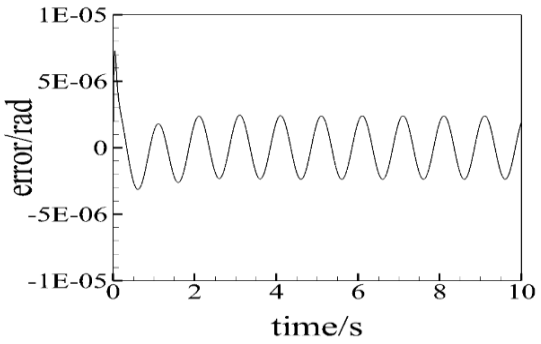

Fig. 9. Tracking error for the friction moment disturbance under the compound axis control

Set the friction moment disturbance as $d_L = 0.2 + 0.1\sin(2\pi t)$ rad. The other disturbance $y = \sin(2\pi t)$ rad. The input of the control system is $u = \sin(t)$ rad. The tracking error of compound axis control is shown in Fig. 10, and the mean square value of tracking error is 4.56×10^{-2} mrad.

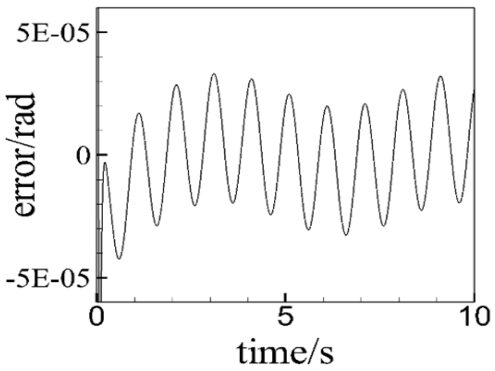

Fig. 10. Tracking error for the multiple disturbances under the compound axis control

In the reference[16], the ratio of the maximum error amplitude to the input signal amplitude is 2.5%, 1.7%, 0.87% under control of the PI controller, automatic digital recording controller (ADRC) and linear active disturbance rejection controller (LADRC), respectively. By using the control method proposed in the paper, the ratio of the maxi-mum error amplitude to the input signal amplitude is 0.005%. But the experiments in this paper are conducted in an ideal environment. The results are more sensitive to the different experimental environments.

3. Coordinate transformation

The attitude of submarine can be determined by the swing angle of submarine deck coordinate system relative to the geodetic coordinate system according to the (the yaw angle α_H, pitching angle α_P, rolling angle α_R). A and E are the azimuth and pitching angle of the target point in the geodetic coordinate system. Due to the small sampling period Δt of CCD, the change of azimuth and pitching angle caused by submarine's translation in unit sampling period is also very small, and the influence of translation motion relative to the ship's rolling motion can be ignored.

Only when the yaw, pitch and roll disturbances occur respectively. The azimuth and pitching angles of the target points $G(x,y,z)$ in the geodetic coordinate system can be solved one by one through α_H, α_P and α_R to the submarine coordinate system. To transfer the coordinates of the target point (X,Y,Z) under the geodetic coordinate system to the submarine coordinate system (X_d,Y_d,Z_d), three steps of the coordinate transformations are needed. (1) The hull rotates at angular speed ω_H around the OZ axis α_H; (2) the hull rotates at angular speed ω_P around the OY axis α_P; (3) the hull rotates at the ω_R around the OX axis α_R.

The solution of these three swing postures can be written in the following matrixes:

$$\begin{bmatrix} X_1 \\ Y_1 \\ Z_1 \end{bmatrix} = \begin{bmatrix} \cos\alpha_P & \sin\alpha_P & 0 \\ -\sin\alpha_P & \cos\alpha_P & 0 \\ 0 & 0 & 1 \end{bmatrix} \begin{bmatrix} X \\ Y \\ Z \end{bmatrix} = T_P \begin{bmatrix} X \\ Y \\ Z \end{bmatrix} \tag{8}$$

$$\begin{bmatrix} X_2 \\ Y_2 \\ Z_2 \end{bmatrix} = \begin{bmatrix} -\cos\alpha_H & 0 & \sin\alpha_H \\ 0 & 1 & 0 \\ -\sin\alpha_H & 0 & \cos\alpha_H \end{bmatrix} \begin{bmatrix} X_1 \\ Y_1 \\ Z_1 \end{bmatrix} = T_H \begin{bmatrix} X \\ Y \\ Z \end{bmatrix} \tag{9}$$

$$\begin{bmatrix} X_d \\ Y_d \\ Z_d \end{bmatrix} = \begin{bmatrix} 1 & 0 & 0 \\ 0 & \cos\alpha_R & \sin\alpha_R \\ 0 & -\sin\alpha_R & \cos\alpha_R \end{bmatrix} \begin{bmatrix} X_2 \\ Y_2 \\ Z_2 \end{bmatrix} = T_R \begin{bmatrix} X \\ Y \\ Z \end{bmatrix} \tag{10}$$

After three coordinate transformations, the hull coordinates are as follows:

$$\begin{bmatrix} X_d \\ Y_d \\ Z_d \end{bmatrix} = T_H T_R T_P \begin{bmatrix} X \\ Y \\ Z \end{bmatrix} = \begin{bmatrix} \cos\alpha_H \cos\alpha_P & \cos\alpha_P \sin\alpha_H & \sin\alpha_P \\ -\sin\alpha_H \cos\alpha_R - \cos\alpha_H \sin\alpha_R \sin\alpha_P & \cos\alpha_H \cos\alpha_R - \sin\alpha_R \sin\alpha_H \sin\alpha_P & \cos\alpha_P \sin\alpha_R \\ -\cos\alpha_H \sin\alpha_P \sin\alpha_R + \sin\alpha_R \sin\alpha_H & -\cos\alpha_H \sin\alpha_R - \sin\alpha_H \sin\alpha_P \cos\alpha_R \cos\alpha_P \cos\alpha_R \end{bmatrix} \begin{bmatrix} X \\ Y \\ Z \end{bmatrix} \tag{11}$$

Converting the rectangular coordinate point of submarine into azimuth and pitching angle in the optical axis coordinate system:

$$\begin{cases} A_{\mathrm{d}} = \arctan\left(Y_{\mathrm{d}} / X_{\mathrm{d}}\right) \\ E_{\mathrm{d}} = \arcsin\left(Z_{\mathrm{d}} / L\right) \end{cases} \tag{12}$$

The L is the slant distance that is the distance between the detection point and the target. The simultaneous equations can be obtained as follows:

$$\begin{cases} A_{\mathrm{d}} = \arctan\{\{\cos E[\cos\alpha_R \sin(A-\alpha_H) - \\ \quad \cos(A-\alpha_H)\sin\alpha_P \sin\alpha_R] + \sin E \times \\ \quad \sin\alpha_R \cos\alpha_P\} \times [\sin E \sin\alpha_P + \\ \quad \cos E \cos\alpha_P \cos(A-\alpha_H)]^{-1}\} \\ E_{\mathrm{d}} = \arcsin\{\cos\alpha_P \cos\alpha_R \sin E - \\ \quad \cos E[\sin\alpha_R \sin(A-\alpha_H) + \\ \quad \sin\alpha_P \cos\alpha_R \cos(A-\alpha_H)\} \end{cases} \tag{13}$$

4. Simulation analysis

4.1. Disturbance solution of submarine propeller

The fluid dynamics disturbance character of submarine is mainly obtained by CFX fluid calculation software. When the submarine is in the navigation state, the disturbance is different from the floating state, the propeller propulsion should be considered. The angle error disturbance in three directions of the visual axis

coordinate system are caused by the interaction between the fluid and the hull, which is finally reflected in the change of the torques in three directions. Through the analysis of the suffering fluid force on the submarine surface around the reference point, the pressure difference moment and viscosity moment in three directions can be obtained. The interference of the fluid on the submarine can be reflected on the torques' changes as well as the visual axis distributions of the photoelectric tracking system.

In the simulation process, the submarine's attitude remains a constant 0 angle of attack and the propeller rotates at a stable speed 150 rev/min. Therefore, the submarine's torque fluctuations can be regarded as the submarine's movement trends. There is a relationship between the torque fluctuation trend and the submarine's angle is the mass and the reference point position. In this study that is approximately considered to be linear. Therefore, this work introduced k_{pv} that is a ratio coefficient for torque and disturbance angle, and its expression can be obtained:

$$k_{pv}=\bar{M}_p+\bar{M}_v \tag{14}$$

$\bar{M}_p$ is the arithmetic mean of the differential pressure torque, $\bar{M}_v$ is the arithmetic mean of the viscous torque. The value of viscosity torque is small and can be ignored. So the scale factor $k_{pv}\approx\bar{M}_p=\sqrt{M_x^2+M_y^2+M_z^2}$, where M_x, M_y, M_z are the moments in three directions obtained by CFD force analysis of submarine. Fig. 11 and Fig. 12 is the torque curves of submarine in three directions and the disturbance diagram of azimuth and pitching of photoelectric tracking system after synthesis. Because the submarine model is not totally symmetrical, there will be non-zero initial values in the three direction torques, so the resultant changes of azimuth and pitching angles are not around 0.

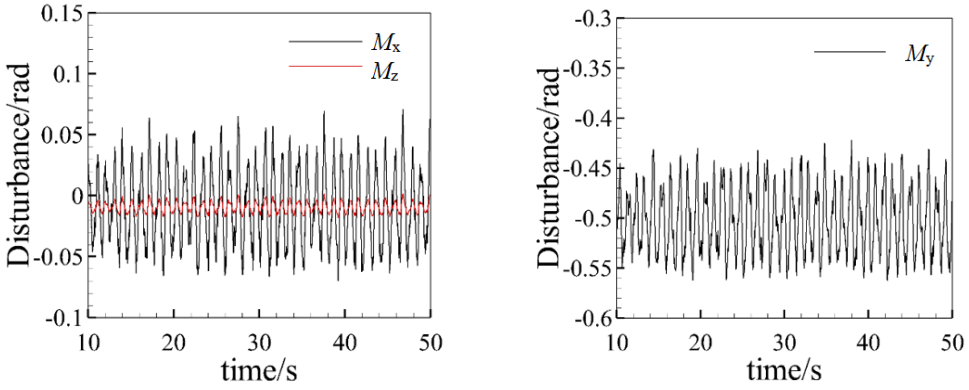

(a) Disturbance curve of moment around the x and z axes

(b) Disturbance curve of moment around the y axis

Fig. 11. Disturbance curves of moment around three directions of submarine

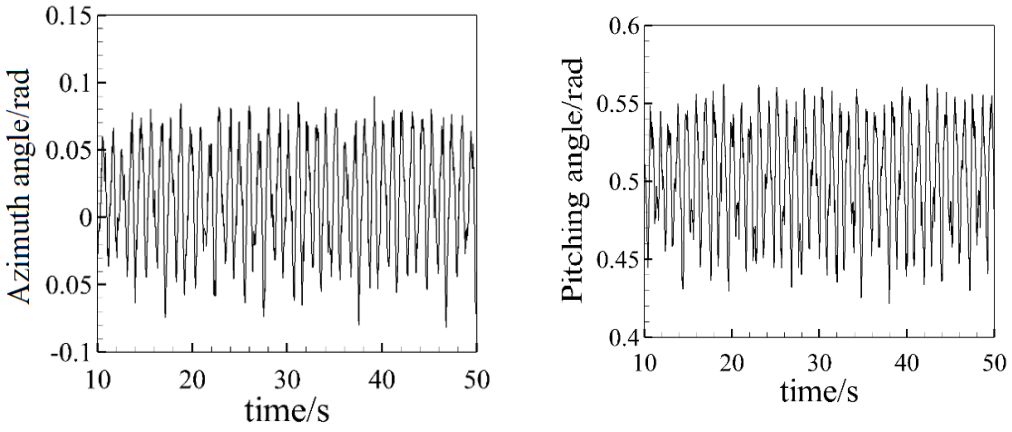

(a) Change curve of the azimuth angle (b) Change curve of the pitching angle

Fig. 12. Change curves of the azimuth and pitching angles in view axis coordinate system

4.2. The disturbance solution caused by the wave

Supposed that the submarine is interfered both by the wave and rotating propeller at a stable speed 150rev/min. And when t=10 s, the target is stationary and centered on the view axis where $A_d = 0$, $E_d = 0$. Affected by the wave, the yaw angle $H(t)$, pitching angle $P(t)$ and roll angle $R(t)$ can be written as:

$$\begin{cases} H(t) = 0.2\sin(1.2t)/\text{rad}; \\ P(t) = 0.12\sin(0.785t)/\text{rad}; \\ R(t) = 0.25\sin(0.628t)/\text{rad}; \end{cases} \tag{15}$$

Due to the instability of the start-up flow field the time of the first 10 seconds have been removed. From t = 10s for normalization, subtract the initial values of A_d (10) and E_d (10) and let A_d、E_d =0 at t=10s. The resulting disturbance is shown in Fig. 13.

The PID controller parameters in fine channel are $K_p = 3$, K_i=200, $K_d = 0.01$. Fractional Order PID parameters are $k_p = 50$, $k_d = 20$, $\mu = 1.3685$, respectively. Nominal model is set to $P(s) = 36.8/s$. Low pass filter $Q(s) = (2\tau s + 1)/(\tau s + 1)^2$, τ=0.001.

The inputs will use the evolution curves value of azimuth and pitching angles in Fig. 13, the mean square value of tracking error of composite axis is shown in Fig. 14. The azimuth error is stable within ±0.8 mrad. The stable pitching error ranges within ±0.6 mrad. The reason for the large error is that the fluid noise from the propeller disturbance is mainly composed of the high frequency disturbance. In the above experimental environments, the ratio of the maximum error amplitude to the input signal amplitude is about 0.2%. It is more

useful in reducing the influence of disturbance.

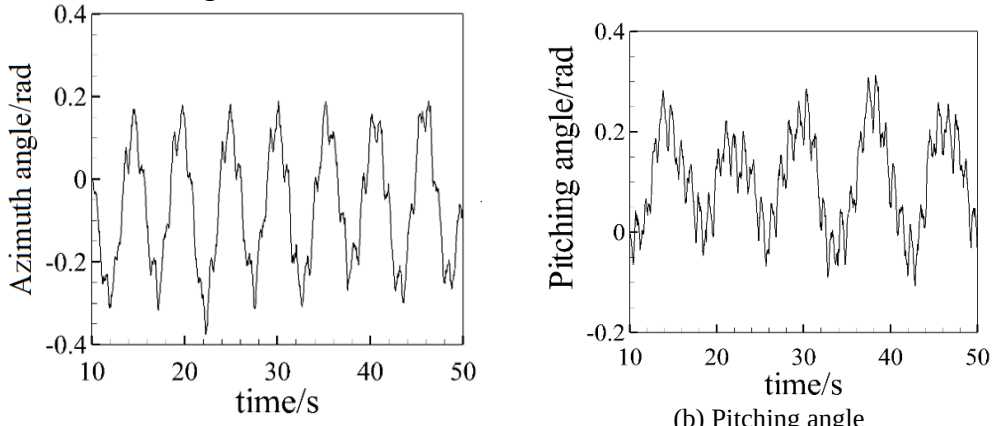

(a) Azimuth angle (b) Pitching angle

Fig. 13. Disturbance curves of the azimuth and pitching angles

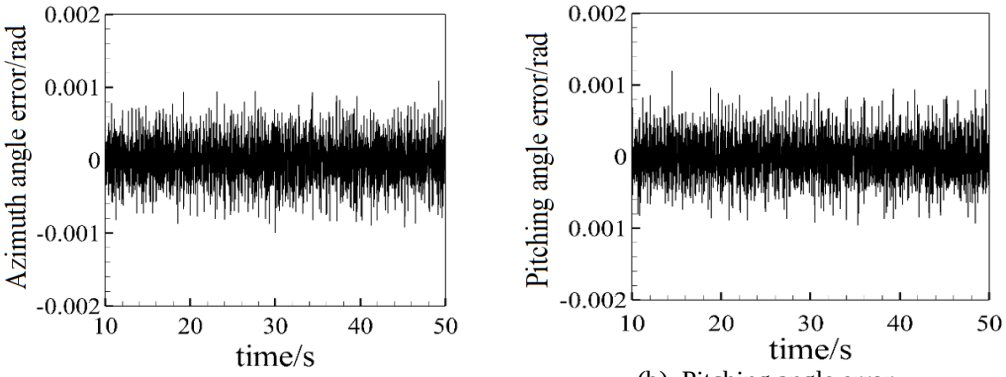

(a). Azimuth angle error (b). Pitching angle error

Fig. 14. The azimuth and pitching angle composite axis tracking errors

5. Conclusions

In this paper, a submarine and a submarine-based compound axis tracking system have been numerical simulated. Firstly, a disturbance observer with fractional order PID control is designed as the coarse tracking controller and the PID controller has been used to adjust the fine channel FSM. Secondly, a submarine navigate in the flow field at 150 rev/min propeller speed is numerical analyzed by CFD software, whose attitude disturbance mainly originated from the propeller propulsion. Based on the submarine hydrodynamic analysis, the moment evolution curves of submarine in three directions around the leading edge point are obtained. Thirdly, combined with the sea wave disturbance, the submarine attitude changes are obtained, and then the azimuth and pitching angle changes of the visual axis are calculated through the coordinate transformation. The simulation results show that this kind of compound axis controller appears a better

effect on suppressing the external disturbance. Finally, the azimuth error is stable at ± 0.8 mrad, and the pitching error is stable at ± 0.6 mrad. It is verified that the designed compound axis control has a good tracking effect. However, due to the disturbance caused by the propeller at this speed, the tracking accuracy is reduced due to a high-frequency small disturbance of the submarine vibration.

Further studies will mainly focus on the application and experiment to examine the improvement of the control strategy. The fluid dynamic numerical researches should be conducted to simulate much more submarine movement or flow field environments, based on which further discusses about the improvement of the control strategies would be given.

Acknowledgments

This project is supported by China Postdoctoral Science Foundation (NO. 2021M691658) and National Natural Science Foundation of China. (NO. 11702139).

R E F E R E N C E S

[1]. *P. H. Leong, S. Arulampalam, T. A. Lamahewa, et al*, A Gaussian Sum Based Cubature Kalman Filter for Bearings Only Tracking, IEEE Transactions on Aerospace and Electronic Systems, **vol. 49**, no. 2, 2013, pp. 1161-1176.

[2]. *Z. K. Liu, F. Zhang,* Research on the optimized control by local Lorentz force to adjust the submarine vibration in the seawater, UPB Scientific Bulletin, **vol. 82**, no. 3, 2020, 51-66.

[3]. *S. C. Amit, W. K. Swapnil, A. S. Junghare, M. V. Aware, D. Shantanu,* Design and Implementation of Digital Fractional Order PID Controller Using Optimal Pole Zero Approximation Method for Magnetic Levitation System, IEEE/CAA Journal of Automatica Sinica, **vol. 5**, no. 05, 2018, 977-989.

[4]. *B. Kar, P. Roy,* A Comparative Study between Cascaded FOPI-FOPD and IOPI-IOPD Controllers Applied to a Level Control Problem in a Coupled Tank System, Journal of Control, Automation and Electrical Systems, **vol. 29**, 2018, pp. 340-349.

[5]. *J. Viola, L. Angel, J. M. Sebastian,* Design and Robust Performance Evaluation of a Fractional Order PID Controller Applied to a DC Moto, IEEE/CAA Journal of Automatica Sinica, **vol. 4**, no. 02, 2017, pp. 304-314.

[6]. *B. Yang, T. Yu, H. C. Shu, Y. M. Han, P. L. Cao, L. Jiang,* Adaptive fractional order PID control of PMSG-based wind energy conversion system for MPPT using linear observers, International Transactions on Electrical Energy Systems, **vol. 29**, no. 1, 2019.

[7]. *S. Seyedtabaii,* New flat phase margin fractional order PID design: Perturbed UAV roll control study, Robotics and Autonomous Systems, 2017, 96.

[8]. *K. Guo, J. H. Wei, J. H. Fang, R. L. Feng, X. C. Wang,* Position tracking control of electro hydraulic single-rod actuator based on an extended disturbance observer, Mechatronics, 2015, 27

[9]. *Y. Caichenga, C. Hongbina, Q. Linfanga, et al.* Adaptive Sliding-Mode Tracking Control for an Uncertain Nonlinear SISO Servo System with a Disturbance Observer, Journal of Shanghai Jiao Tong University (Science), **vol. 23**, no. 03, 2018, pp. 376-383.

[10]. *M. Chen,* Robust Tracking Control for Self-balancing Mobile Robots Using Disturbance

Observer, IEEE/CAA Journal of Automatica Sinica, **vol. 4**, no. 03, 2017, pp. 458-465.
[11]. *M. Chen, W. H. Chen, Q. X. Wu,* Adaptive fuzzy tracking control for a class of uncertain MIMO nonlinear systems using disturbance observer, Science China (Information Sciences), **vol. 57**, no. 01, 2014, pp. 246-258.
[12]. *A. Aishwarya, T. Ujjwala, J. Vrunda,* Disturbance Observer Based Speed Control of PMSM Using Fractional Order PI Controller, IEEE/CAA Journal of Automatica Sinica, **vol. 6**, no. 01, 2019, pp. 316-326.
[13]. *H. S. Lee, M. Tomizuka,* Robust motion controller design for high-accuracy positioning systems, IEEE Transactions on Industrial Electronics, **vol. 43**, no. 1, 1996, pp. 48-55.
[14]. *K. J. Åström, B. Wittenmark,* Computer-controlled systems: theory and design, Courier Corporation, 2013, pp. 345-375.
[15]. *D. Valério, I. Tejado,* Identifying a non-commensurable fractional transfer function from a frequency response, Elsevier B.V. 2015, pp. 254-264.
[16]. *W. Wanting, J. Guo, Z. H. Jiang, T. F. Wang,* Application of linear active disturbance rejection control for photoelectric tracking system, High Technology Letters, **vol. 23**, no. 03, 2017, pp. 315-321.